Ultrafast Optical Control of the Electronic Properties of $ZrTe_5$

G. Manzoni,[1] A. Sterzi,[1] A. Crepaldi,[2,*] M. Diego,[1] F. Cilento,[2] M. Zacchigna,[3] Ph. Bugnon,[4] H. Berger,[4] A. Magrez,[4] M. Grioni,[4] and F. Parmigiani[1,2,5]

[1]*Universitá degli Studi di Trieste, Via A. Valerio 2, Trieste 34127, Italy*

[2]*Elettra-Sincrotrone Trieste S. C. p. A., Strada Statale 14, km 163.5, 34149 Basovizza, Trieste, Italy*

[3]*C.N.R.-I.O.M., Strada Statale 14, km 163.5, 34149 Trieste, Italy*

[4]*Institute of Condensed Matter Physics, Ecole Polytechnique Fédérale de Lausanne (EPFL), CH-1015 Lausanne, Switzerland*

[5]*International Faculty, University of Köln, 50937 Köln, Germany*

(Received 3 July 2015; revised manuscript received 14 September 2015; published 10 November 2015)

We report on the temperature dependence of the $ZrTe_5$ electronic properties, studied at equilibrium and out of equilibrium, by means of time and angle resolved photoelectron spectroscopy. Our results unveil the dependence of the electronic band structure across the Fermi energy on the sample temperature. This finding is regarded as the dominant mechanism responsible for the anomalous resistivity observed at $T^* \sim 160$ K along with the change of the charge carrier character from holelike to electronlike. Having addressed these long-lasting questions, we prove the possibility to control, at the ultrashort time scale, both the binding energy and the quasiparticle lifetime of the valence band. These experimental evidences pave the way for optically controlling the thermoelectric and magnetoelectric transport properties of $ZrTe_5$.

DOI: 10.1103/PhysRevLett.115.207402 PACS numbers: 78.47.J-, 73.20.-r, 79.60.-i

Transition metal pentatelluride $ZrTe_5$ displays a rich set of unique and exotic transport properties that make this material an emerging candidate for magnetic and thermoelectric devices [1,2]. The complexity of the $ZrTe_5$ electronic properties has become clear since its first synthesis in 1973 [3]. The thermopower changes sign from positive to negative when cooling down across T^* [4], meanwhile the resistivity increases by a factor ~3 [5], and the charge carrier switches from holes, at $T > T^*$, to electrons, for $T < T^*$ [6]. Several models have been proposed to interpret these transport properties, based on charge density wave [4] or polaron [7] formation, but so far they are not supported by direct experimental evidence [8,9].

The discovery of large magnetoresistance, with both positive [10] and, more surprisingly, negative sign [11], has proved that the magnetic and electronic transport properties are tightly connected in $ZrTe_5$. These findings have been recently regarded as a sign of chiral magnetic effect, possible in the case of 3D Dirac semimetal [11–14]. Furthermore, $ZrTe_5$ exhibits a superconducting state under pressure [15] while spin helical surface states have also been predicted [16,17]. All together, these properties require further thorough investigation of the physical properties of this material, with particular attention to the interplay between temperature and electronic structure, with the aim to clarify the still unknown origin of the resistivity anomaly.

In this Letter, by combining angle resolved photoelectron spectroscopy (ARPES) and time resolved ARPES (tr-ARPES), we unveil the evolution of the electronic structure versus temperature in $ZrTe_5$. Moreover, by studying the out-of-equilibrium band structure, we prove the possibility of optically controlling the electronic properties of $ZrTe_5$. All together, our findings indicate the way to manipulate, at the ultrashort time scale, both the thermoelectric and magnetoelectric transport properties.

One of the key points of our experiment is the direct imaging of the conduction band (CB). This band, located above the Fermi level (E_F), is transiently populated and detected via a nonlinear two-photon photoemission (2PPE) process. Temperature-dependent experiments reveal a negative energy shift of the $ZrTe_5$ band structure. The same binding energy shift is observed also by optically exciting the system out of equilibrium. The combined knowledge of both the occupied and unoccupied band structure, along with its temporal evolution across T^*, enables us to account for the origin of the anomalous resistivity peak and the charge carrier switch from holes, at $T > T^*$, to electron, at $T < T^*$. Having clarified the electronic mechanisms that control the transport properties in $ZrTe_5$, we prove that, by means of an ultrafast optical excitation, it is possible to directly control the energy position of the band structure and the quasiparticle lifetime in the occupied valence band (VB) states.

The tr-ARPES experiments are performed at the T-ReX Laboratory, Elettra (Trieste, Italy), operating a Ti:sapphire regenerative amplifier (Coherent RegA 9050) working at 250 kHz repetition rate, whose laser fundamental emission centered at 800 nm (~1.55 eV) is split into two beams. The p-polarized pump beam excites the $ZrTe_5$ samples with an impinging fluence ~100 $\mu J/cm^2$. Electrons are photoemitted by the probe beam, corresponding to the laser 4th harmonic (~6.2 eV) generated in phase-matched barium borate (BBO) crystals. A $\lambda/2$ wave plate is used for setting

the *s*- or *p*-polarization state for the probe beam. The photoelectrons are collected and analyzed by a SPECS Phoibos 225 hemispherical spectrometer, with energy and angular resolution set to 10 meV and 0.2°, respectively. The overall temporal resolution is equal to 250 fs [18]. High quality $ZrTe_5$ single crystals are grown by a direct vapor transport technique with iodine methods [19]. The samples are cleaved in ultrahigh vacuum and mounted on a variable temperature cryostat. The precise temperature of the resistivity anomaly slightly depends on the sample growth conditions [7], and for the present study it corresponds to $T^* \sim 160$ K [20].

$ZrTe_5$ crystallizes in the layered orthorombic crystal structure and it belongs to the $Cmcm(D_{2h}^{17})$ point group, as shown in Fig. 1(a), as taken from Ref. [16]. Each primitive unit cell contains two $ZrTe_3$ chains (Zr in blue and Te2 in black) linked along the *c* direction by two zigzag chains formed by Te1 atoms (in red) [16,21]. The resulting $ZrTe_5$ planes are stacked along the *b* axis, bound by van der Waals forces, resulting in very small interlayer binding energy, comparable to the one of graphite [16]. Crystals grow naturally oriented along the *a* axis exposing the *ac* plane. The low-dimensional nature of the prismatic chains and the weak interlayer binding energy sometimes leave the cleaved surface with multiple domains characterized by different out-of-plane chain orientations. Hence, particular attention is required during ARPES measurements (for more details, see the Supplemental Material [22]).

We have investigated in detail the temperature evolution of the electronic band structure of $ZrTe_5$ along the chain direction, corresponding to the ΓX high symmetry direction in the reciprocal space (with $\Gamma X = 0.78$ Å^{-1}). Owing to the low photon energy (6.2 eV), only states close to Γ (± 0.13 Å^{-1}) are resolved. However, previous ARPES experiments [11], band structure calculations [16], and Shubnikov–de Haas studies [23] show that the maximum of the valence band and the minimum of the conduction band are located at the Γ point and disperse close to E_F. Hence,

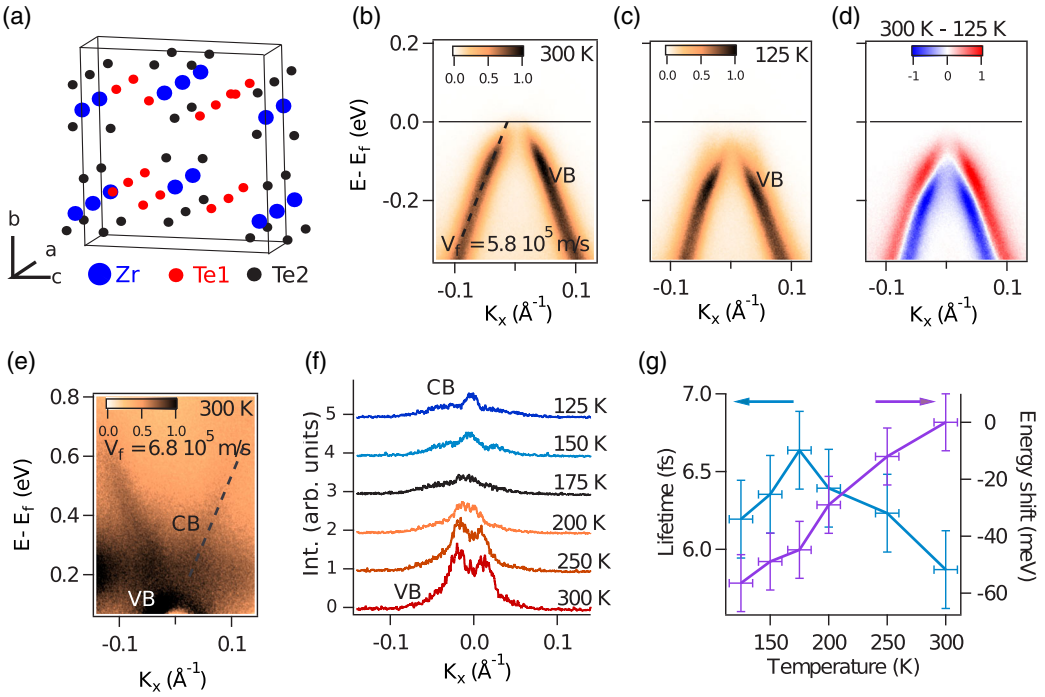

FIG. 1 (color online). (a) Schematic of the $ZrTe_5$ crystal structure, formed by chains of $ZrTe_3$ (Zr in blue and Te2 in black), running along the *a* crystallographic direction and linked along the *c* direction by zigzag chains formed by Te1 atoms (in red) [16,21]. (b), (c) Electronic band structure of $ZrTe_5$ along the chain direction ΓX measured at 300 and 125 K respectively, using *s*-polarized light. A linear fit of the valence band (VB) dispersion, dashed line in (b), results in a band velocity equal to $\sim 5.8 \times 10^5$ m/s. (d) Difference image obtained by subtracting the low temperature band dispersion from the high temperature. Blue and red indicate the transfer of spectral weight to lower energies when cooling down. (e) Unoccupied conduction band (CB), probed with *p*-polarized light after optical transfer of charges from the occupied VB. The band velocity, extracted from a linear fit, corresponds to $\sim 6.8 \times 10^5$ m/s. (f) Evolution of the spectral weight in proximity of the Fermi level E_F. MDCs are integrated 20 meV below E_F and positively shift along the vertical axis for the different sample temperatures. The spectrum evolves from the double peaks of the VB crossing E_F at room temperature, to a minimum of intensity at 175 K, followed by an increase of intensity which we attribute to the appearance of CB at lower temperature. (g) Evolution of the binding energy shift and the quasiparticle lifetime as extracted from the fit of the MDCs as a function of the temperature. The increasing lifetime from room temperature to 175 K is a signature of metallic behavior, whereas at temperatures lower than 175 K the lifetime decreases, indicating an increased scattering rate when the VB state lies completely below E_F.

only these states are responsible for the electronic transport properties. A remarkable shift of the band towards lower energies is detected upon cooling, as extracted from the analysis of the momentum distribution curves (MDCs) (for more details, see the Supplemental Material [22]). Results at equilibrium are summarized in Fig. 1. Figures 1(b) and 1(c) show the ARPES images of the VB, dispersing with negative effective mass, measured with s-polarized light at 300 and 125 K, respectively. The VB is found to cross E_F, and the Fermi wave vector k_F decreases at lower temperatures, consistently with data reported in Ref. [24]. Figure 1(g) quantifies the magnitude of the energy shift in the investigated temperature range (300–125 K), with a maximum value equal to $\sim 60 \pm 10$ meV. Figure 1(d) shows the difference image, obtained by subtracting the band dispersion at $T = 125$ K from that at $T = 300$ K. This procedure provides a direct visualization of the energy shift and a comparison with the out-of-equilibrium tr-ARPES results, discussed later.

In order to explain the mechanism at the origin of the $ZrTe_5$ anomalous transport properties, it is also necessary to access the unoccupied band structure, whose contribution becomes relevant when new bands approach E_F at temperature close to T^*. In order to study the band dispersion of the unoccupied CB, two-photon photoemission experiments are used. Following this scheme, the laser optical excitation transiently populates the CB, which is at the same time probed by an ultrafast laser UV pulse [25,26]. 2PPE results are interpreted as the projection of the initial state onto intermediate unoccupied states below the vacuum level. Figure 1(e) shows the results of 2PPE experiments with p-polarized light. The intensity is almost completely suppressed in measurements with s-polarized light. Since the VB disperses around Γ with a negative effective mass, the observed positive dispersion is ascribed to the CB, in agreement with *ab initio* calculations [16]. A linear fit of the band dispersion, dashed line, results in a band velocity of $\sim 6.8 \times 10^5$ m/s, which is close to the $\sim 5.8 \times 10^5$ m/s band velocity obtained for the VB. These comparable band velocities leave open the possibility to describe these states in terms of linearly dispersing 3D Dirac particles, as recently proposed [11]. Our data are compatible with an energy gap not larger than $\sim 50 \pm 10$ meV, comparable with the observed energy shift.

Figure 1(f) shows the evolution of the intensity at E_F as a function of temperature. MDCs are integrated in an energy window of 20 meV below E_F and displayed with a vertical offset. At $T = 300$ K (bottom curve), we clearly distinguish the double peak structure of the VB crossing E_F. Upon cooling, the two peaks get closer and eventually merge, indicating that the top of the VB lies below E_F. The minimum of intensity is observed at 175 K, close to the resistivity peak located at $T^* = 160$ K. At lower temperature, a new peak appears. This increase of spectral weight is attributed to the lowering of the CB below E_F. Finally, Fig. 1(g) shows, along with the energy shift, the temperature evolution of the quasiparticle lifetime τ_l extracted from the Lorentzian fit of the MDCs (for more details, see the Supplemental Material [22]). Between 300 and 175 K, τ_l increases with decreasing temperature, as expected for a metal. Conversely, below $T < 175$ K, τ_l monotonically decreases. This is regarded as the signature of an increased electron scattering rate as VB is fully occupied.

Having clarified the origin of the anomalous behavior of the resistivity and the nature of the charge carriers across T^*, we now prove the possibility to control the electronic properties of $ZrTe_5$ by means of an ultrafast optical pulse. Figure 2 shows the electronic properties (a) for an equilibrium lattice temperature of 125 K before the arrival of the optical perturbation (−800 fs), and (b) the difference

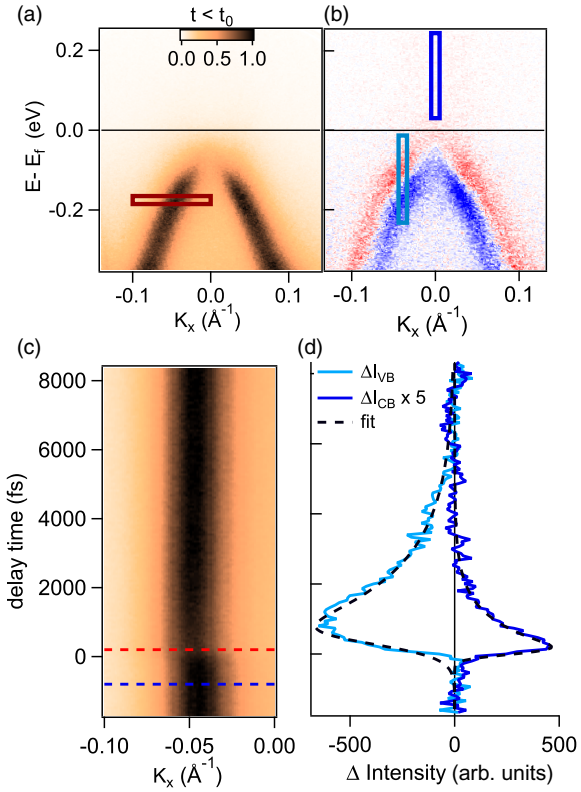

FIG. 2 (color online). (a) Equilibrium electronic structure of $ZrTe_5$ measured along the chain direction with s-polarized light at 125 K before optical excitation (−800 fs). (b) Difference image between the data acquired immediately after (200 fs) and before (−800 fs) optical excitation. The color scale provides a direct comparison with Fig. 1(d). The close similarity suggests to interpret the results in term of a band energy shift accompanied by the increased temperature after optical perturbation. (c) Temporal evolution of the MDCs at −0.2 eV in the momentum window within the red rectangle of (a). (d) Temporal dynamics of the electron population in CB and VB, as integrated in the rectangles of (b). The traces are fitted (black dashed lines) with a single decaying exponential, resulting in different characteristic times for CB, $\tau_{CB} = 0.8 \pm 0.2$ ps, and VB $\tau_{VB} = 1.6 \pm 0.2$ ps.

between the data immediately after (200 fs) and before (−800 fs) the arrival of the pump pulse. Figure 2(b) displays a large energy shift of the bands very similar to that shown in Fig. 1(c), which we interpret as follows. The optical excitation is responsible for two intertwined effects: the charge excitation from VB to CB, and the increase in the electronic energy. The latter results in the increase of both the electronic and lattice temperatures, hence accounting for the energy shift of the band structure. However, few fs temporal resolution would be necessary to disentangle the electronic contribution from the lattice one. Figure 2(c) shows the evolution of the MDCs at $E - E_F = -0.2$ eV for $-0.1 < k < 0$ Å^{-1} in the region highlighted with the rectangle in Fig. 2(a). This small momentum window is chosen in order to better visualize the dynamics of the band shift as a consequence of the transient increase in temperature.

One of the key results reported in this Letter is the capability to manipulate, at the ultrashort time scale, the electronic band structure of $ZrTe_5$. At the same time, we also report on the dynamics of the charge transfer between VB and CB. Figure 2(d) shows the temporal evolution of the electron population in VB (negative signal) and CB (positive signal) integrated in the energy-momentum windows enclosed by rectangles in Fig. 2(b). The integration windows are chosen in order to account in the same momentum window for the energy shift of the band. A single decaying exponential fit of the CB dynamics gives a characteristic time $\tau_{CB} = 0.8 \pm 0.2$ ps, which is significantly different from $\tau_{VB} = 1.6 \pm 0.2$ ps measured for VB. We notice also that the maximum excitation in the VB is delayed with respect to the CB. These findings indicate that different scattering mechanisms are responsible for both the electron (hole) accumulation at the bottom (top) of the CB (VB) and the subsequent relaxation.

Figure 3 summarizes the dynamics of the optically induced band energy shift. We compare the temporal dynamics of the MDCs measured at an equilibrium lattice temperature of 125 (blue) and 300 K (red). For these two temperatures, the MDCs are extracted at −0.2 and −0.14 eV, respectively, in order to compare the dynamics of the emission peak at the same k value. Figure 3(a) shows, with a vertical offset, two MDCs for an equilibrium lattice temperature of 125 K before (−800 fs, dark blue) and after optical excitation (200 fs, light blue), along with the best fit (black line). Each MDC is fitted with a double Lorentzian function plus a polynomial background, as for the analysis in Fig. 1. From each fit we obtain the temporal evolution of the Lorentzian function parameters: intensity, position of the maximum, and width. Hereafter, we limit the discussion to the results for the band branch at negative k values. Figure 3(b) shows the evolution of the intensity, normalized to the value at equilibrium. The intensity decreases after optical excitation as a consequence of the combined increase in temperature (broadening of the Fermi Dirac distribution) and the charge excitation from VB to CB. Figure 3(c) shows the dynamics of the maximum intensity position, which shifts to larger momentum values reflecting the band energy shift.

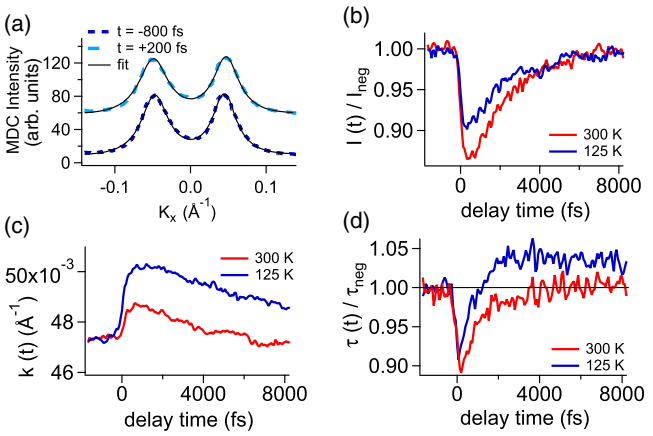

FIG. 3 (color online). (a) MDCs extracted for a lattice temperature at equilibrium of 125 K at −0.2 eV, as measured before (−800 fs, dark blue) and after (200 fs, light blue) optical excitation, displayed with a vertical offset. The best-fit curves (black lines) are obtained with a double Lorentzian function plus a polynomial background. (b)–(d) Results of the analysis of the Lorentzian fit to the MDCs as extracted at −0.2 eV (blue, 125 K) and −0.14 eV (red, 300 K). The two energies are chosen in order to compare the band peak dynamics at the same k position. (b) Dynamics of the left Lorentzian peak intensity at 300 and 125 K, normalized to the negative time values. (c) Comparison between the peak positions, reflecting the band energy shift. (d) Temporal evolution of the quasiparticle lifetime τ_l. A significant increase in lifetime is observed for long delay time, only for the equilibrium lattice temperature of 125 K.

Finally, we focus on the Lorentzian width, which is expressed in terms of the quasiparticle lifetime τ_l, normalized to the value before optical excitation. In stark contrast to the intensity and maximum intensity position, which have qualitatively the same dynamics for both $T = 300$ and 125 K, τ_l shows different behaviors for the two different equilibrium lattice temperatures. At short time scale, both at 300 and 125 K, τ_l shortens after optical excitation. While at 300 K, τ_l recovers its equilibrium value with a single decaying exponential, with characteristic time 1.1 ps, at 125 K τ_l changes sign and increases by ∼5% of the equilibrium value. The observed increase in the quasiparticle lifetime is consistent with the increase in the electronic and lattice temperature, as shown in Fig. 1(g).

In conclusion, in this Letter we report a comprehensive investigation of both the occupied (VB) and unoccupied (CB) states of $ZrTe_5$ revealing a binding energy shift of these bands as a function of temperature. This remarkable finding unveils the origin of the resistivity anomaly at $T^* \sim 160$ K along with the charge carriers' switch from holes to electrons upon decreasing the temperature across T^*. Having clarified the mechanism at the origin of the

transport anomaly of $ZrTe_5$, we have experimentally proven the possibility to optically modify the electronic properties of this material both in terms of binding energy and quasiparticle lifetime of the valence band, thus leading to the control, at the ultrafast time scale, of the transport properties of $ZrTe_5$. These results provide an external knob to control the $ZrTe_5$ conductivity and to unlock the route for a unique platform for magnetoelectric, optical, and thermoelectric transport applications.

Very recently, we became aware that a similar effect of temperature-dependent energy shift of the electronic band structure has been reported by ARPES experiments on WTe_2 [27], a material that also displays unique electronic properties [28]. This suggests that the mechanism studied in this Letter is general and of fundamental importance in controlling the transport properties of a potentially wide class of materials.

This work was supported in part by the Italian Ministry of University and Research under Grants No. FIRBRBAP045JF2 and No. FIRB-RBAP06AWK3, and by the European Community Research Infrastructure Action under the FP6 "Structuring the European Research Area" Program through the Integrated Infrastructure Initiative "Integrating Activity on Synchrotron and Free Electron Laser Science," Contract No. RII3-CT-2004-506008. We acknowledge support by the Swiss NSF.

*alberto.crepaldi@elettra.eu

[1] T. Sambongi, in *Physics and Chemistry of Materials with Low-Dimensional Structures* (Springer, Netherlands, 1986), Vol. 5.
[2] T. M. Tritt and R. T. Littleton IV, in *Semiconductors and Semimetals* (Elsevier, 2001), Vol. 70, Chap. 6.
[3] S. Furuseth, L. Brattas, and A. Kjejshus, Acta Chem. Scand. **27**, 2367 (1973).
[4] T. E. Jones, W. W. Fuller, T. J. Wieting, and F. Levy, Solid State Commun. **42**, 793 (1982).
[5] E. F. Skelton, T. J. Wieting, S. A. Wolf, W. W. Fuller, D. U. Gubser, T. L. Francavilla, and F. Levy, Solid State Commun. **42**, 1 (1982).
[6] M. Izumi, K. Uchinokura, E. Matsuura, and S. Harada, Solid State Commun. **42**, 773 (1982).
[7] M. Rubinstein, Phys. Rev. B **60**, 1627 (1999).
[8] F. J. DiSalvo, R. M. Fleming, and J. V. Waszczak, Phys. Rev. B **24**, 2935 (1981).
[9] S. Okada, T. Sambongi, M. Ido, Y. Tazuke, R. Aoki, and O. Fujita, J. Phys. Soc. Jpn. **51**, 460 (1982).
[10] T. M. Tritt, N. D. Lowhorn, R. T. Littleton, A. Pope, C. R. Feger, and J. W. Kolis, Phys. Rev. B **60**, 7816 (1999).
[11] Q. Li, D. E. Kharzeev, C. Zhang, Y. Huang, I. Pletikosic, A. V. Fedorov, R. D. Zhong, J. A. Schneeloch, G. D. Gu, and T. Valla, arXiv:1412.6543.
[12] P. J. Moll, N. L. Nair, T. Helm, A. C. Potter, I. Kimchi, A. Vishwanath, and J. G. Analytis, arXiv:1505.02817v1.
[13] R. Y. Chen, S. J. Zhang, J. A. Schneeloch, C. Zhang, Q. Li, G. D. Gu, and N. L. Wang, Phys. Rev. B **92**, 075107 (2015).
[14] R. Y. Chen, Z. G. Chen, X.-Y. Song, J. A. Schneeloch, G. D. Gu, F. Wang, and N. L. Wang, Phys. Rev. Lett. **115**, 176404 (2015).
[15] Y. Zhou, W. Ning, Y. Du, Z. Chi, X. Chen, X. Wang, X. Zhu, X. Wan, Z. Yang, M. Tian *et al.*, arXiv:1505.02658.
[16] H. Weng, X. Dai, and Z. Fang, Phys. Rev. X **4**, 011002 (2014).
[17] M. Z. Hasan and C. L. Kane, Rev. Mod. Phys. **82**, 3045 (2010).
[18] A. Crepaldi, B. Ressel, F. Cilento, M. Zacchigna, C. Grazioli, H. Berger, P. Bugnon, K. Kern, M. Grioni, and F. Parmigiani, Phys. Rev. B **86**, 205133 (2012).
[19] F. Lévy and H. Berger, J. Cryst. Growth **61**, 61 (1983).
[20] J. C. Johannsen (private communication).
[21] H. Fjellvag and A. Kjejshus, Solid State Commun. **60**, 91 (1986).
[22] See Supplemental Material at http://link.aps.org/supplemental/10.1103/PhysRevLett.115.207402 for more details about the data analysis and the photoemission results.
[23] G. N. Kamm, D. J. Gillespie, A. C. Ehrlich, T. J. Wieting, and F. Levy, Phys. Rev. B **31**, 7617 (1985).
[24] D. N. McIlroy, S. Moore, D. Zhang, J. Wharton, B. Kempton, R. Littleton, M. Wilson, T. M. Tritt, and C. G. Olson, J. Phys. Condens. Matter **16**, L359 (2004).
[25] J. C. Johannsen, G. Autès, A. Crepaldi, S. Moser, B. Casarin, F. Cilento, M. Zacchigna, H. Berger, A. Magrez, P. Bugnon *et al.*, Phys. Rev. B **91**, 201101 (2015).
[26] J. A. Sobota, S.-L. Yang, A. F. Kemper, J. J. Lee, F. T. Schmitt, W. Li, R. G. Moore, J. G. Analytis, I. R. Fisher, P. S. Kirchmann *et al.*, Phys. Rev. Lett. **111**, 136802 (2013).
[27] Y. Wu, N. H. Jo, M. Ochi, L. Huang, D. Mou, S. L. Budko, P. C. Canfield, N. Trivedi, R. Arita, and A. Kaminski, Phys. Rev. Lett. **115**, 166602 (2015).
[28] M. N. Ali, J. Xiong, S. Flynn, J. Tao, Q. D. Gibson, L. M. Schoop, T. Liang, N. Haldolaarachchige, M. Hirschberger, N. P. Ong *et al.*, Nature (London) **514**, 205 (2014).